Journal of Magnetic Resonance 193 (2008) 10–22

Contents lists available at ScienceDirect

Journal of Magnetic Resonance

journal homepage: www.elsevier.com/locate/jmr

Probing the validity of average Hamiltonian theory for spin $I = 1, 3/2$ and $5/2$ nuclei by analyzing a simple two-pulse sequence

E.S. Mananga [a,b], C.D. Hsu [c], S. Ishmael [a], T. Islam [a], G.S. Boutis [a,*]

[a] York College, The City University of New York, Department of Earth and Physical Sciences, 94-20 Guy R. Brewer Boulevard, Jamaica, NY 11451, USA
[b] The Graduate Center of The City University of New York, OEODP, 365 Fifth Avenue, New York, NY 10016-4309, USA
[c] Queens High School for the Sciences at York College, 94-50 159th Street, Jamaica, NY 11451, USA

ARTICLE INFO

Article history:
Received 3 December 2007
Revised 19 March 2008
Available online 3 April 2008

Keywords:
Quadrupolar echo
Finite pulse widths
Average Hamiltonian theory

ABSTRACT

In this work, we investigate the accuracy of controlling spin $I = 1, 3/2$ and $5/2$ spin systems by average Hamiltonian theory. By way of example, we consider a simple two-pulse echo sequence and compare this perturbation scheme to a numerical solution of the Von Neumann equation. For the different values of I, we examine this precision as a function of the quadrupolar coupling as well as various experimental parameters such as the pulse spacing and pulse width. Experiments and simulations on $I = 3/2$ and $I = 5/2$ spin systems are presented that highlight a spectral artifact introduced due to finite pulse widths as predicted by average Hamiltonian theory. The control of these spin systems by this perturbation scheme is considered by investigating a phase cycling scheme that suppresses these artifacts to zeroth-order of the Magnus expansion.

1. Introduction

The ability to control the dynamics of nuclear spins has been of general interest to the NMR community since the early days of the field [1]. A celebrated example is Hahn's demonstration of the refocusing of spin magnetization by the application of a suitable RF pulse sequence as nuclear spins of a liquid dephased due to static field inhomogeneity [2]. Numerous examples of improving quantum control in NMR are known within the community, such as enhanced radio frequency pulses that precisely implement a desired system evolution [3–8]. The aim of the work presented here is to study average Hamiltonian theory (AHT), developed by Waugh and Haeberlen [9], as a viable perturbation scheme for controlling the complex spin dynamics for an ensemble of spin $I = 1, 3/2$ and $5/2$ nuclei of a solid evolving under the first-order quadrupolar interaction for a simple two-pulse sequence.

A well known study that probed the validity of AHT was reported on by Maricq for spin $I = 1/2$ nuclei coupled via the dipolar interaction [10]. In that work, a perturbation expansion is implemented from Floquet theory that gives an average Hamiltonian equivalent to that obtained from a Magnus expansion whose convergence is shown to depend on a series of resonances. The investigation of the spin dynamics of nuclei with $I > 1$ poses a theoretical challenge because the dimension of the density matrix increases with I as $(2I + 1)(2I + 1)$. In addition, the strength of the quadrupolar coupling for such spin systems is often the same order of magnitude as the perturbing RF Hamiltonian. Thus implementing a desired evolution is challenging in both theory and practice. In this work, we focus on a simple two-pulse cycle and investigate the relative accuracy of first-order AHT compared to a numerical result obtained from the Louiville Von Neumann (VN) equation. While this simple cycle is useful for echo spectroscopy of quadrupolar spins, it also forms the basis of many homonuclear multiple-pulse decoupling schemes, such as WAHUHA and MREV-8, that allow for spectroscopic studies of solids [11].

I. Solomon first reported on multiple spin echoes he observed in KI and analyzed the spin dynamics ignoring the quadrupolar interaction during the RF pulses [12]. By accounting for the system evolving under the first-order quadrupolar interaction during the RF pulses, Man reported on multiple quantum coherence detected in echo spectroscopy of spin $I = 5/2$ nuclei [13] and the suppression of spurious artifacts in spin $I = 3/2$ nuclei acquired by this pulsed scheme [14]. Haase and Oldfield investigated spin relaxation and linewidths of a variety of non-integer spins using an echo experiment and provided an analysis that accounts for the evolution of the spin system under the first-order quadrupolar interaction during the RF pulses [15]. Nagel et al. have also reported on a density matrix calculation of spin echoes for spin 5/2 nuclei [16], and Pandey et al. reported on the pulsed NMR signal of spin $I = 3/2$ nuclei [17].

The simulation study of this work probes the validity of AHT for a simple two-pulse sequence for an ensemble of either $I = 1, 3/2$ or $5/2$ spin systems. This is achieved by comparing the results obtained by this analysis to an exact solution obtained computation-

* Corresponding author. Fax: +1 718 262 2652.
E-mail address: gboutis@york.cuny.edu (G.S. Boutis).

1090-7807/$ - see front matter © 2008 Published by Elsevier Inc.
doi:10.1016/j.jmr.2008.03.014

ally solving the VN equation. Dumazy et al. [18] described an optimum phase cycle for a system of spin $I = 3/2$ nuclei that removes ill-refocused echoes, anti-echoes and transient signals. The analysis presented here is also used to predict a spectral distortion in the spectra of spin $I = 1, 3/2$ and $5/2$ nuclei acquired under this simple two-pulse cycle. The work we present also highlights a phase cycling scheme that to first-order of the Magnus expansion suppresses this distortion, and experimental and simulation results are presented demonstrating the efficacy of this technique.

2. Theory

Consider an ensemble of quadrupolar spins of a solid subject to a high magnetic field. The first-order secular quadrupolar interaction is given by

$$H_Q = \omega_Q[3I_zI_z - II] \tag{1}$$

where

$$\omega_Q = \frac{e^2qQ}{2I(2I-1)\hbar\sqrt{6}}\sqrt{\frac{3}{2}}\left[P_2(\cos(\theta)) + \left(\frac{\eta}{2}\right)\cos(2\theta)\sin^2(\varphi)\right] \tag{2}$$

In the above equations, ω_Q is the quadrupolar splitting, and $P_2(\cos(\theta))$ is the second-order Legendre polynomial of $\cos(\theta)$, θ and φ are the usual Euler angles and η is the quadrupolar asymmetry parameter.

In the following, we analyze the evolution of a solid system evolving under the pulse sequence shown in Fig. 1 which consists of two $\pi/2$ phase shifted pulses separated by a delay $\tau - 2\alpha$, where 2α is the $\pi/2$ pulse width. Our goal is to investigate the validity of AHT for an ensemble of spin $I = 1, 3/2$ and $5/2$ nuclei as a function of ω_Q, τ and α. Following the comparison of AHT to the VN solution, we show how cycling the phases of the receiver in a well-defined way can suppress artifacts in the spectra due to the evolution of the system under H_Q during the applied radio frequency pulses.

In the AHT approach, a time-dependent Hamiltonian of the system over one cycle is replaced by an equivalent time-independent average Hamiltonian. The time evolution of the system from time $t = 0$, $\rho(0)$, to the state at time $t = t_c$, $\rho(t_c)$, is given by

$$\rho(t_c) = U_{RF}U_{int}\rho(0)U_{int}^{-1}U_{RF}^{-1} \tag{3}$$

where U_{int} is given by the Magnus expansion

$$U_{int}(t_c, 0) = \exp\left[-it_c(\overline{H}^0_{int} + \overline{H}^1_{int} + \cdots)\right] \tag{4}$$

with

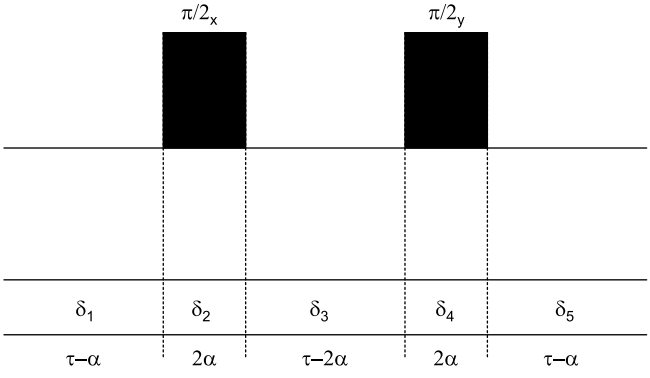

Fig. 1. A two-pulse sequence for refocusing the quadrupolar Hamiltonian. In the figure, the two $\pi/2$ pulses have a width of 2α. The phases of the two-pulses shown for the purposes of this work can be any combination of phase shifted 90 degree pulses.

$$\overline{H}^0_{int} = \frac{1}{t_c}\int_0^{t_c}\widetilde{H}_{int}(t)\,dt \tag{5}$$

$$\overline{H}^1_{int} = \frac{-i}{2t_c}\int_0^{t_c}\left[\widetilde{H}_{int}(\tau), \int_0^{\tau}\widetilde{H}_{int}(\phi)d\phi\right]d\tau \tag{6}$$

The propagator U_{RF} represents the interaction associated with the sequence of RF pulses applied over a time t_c and accounts for the rotations imparted to the system. The rotation operator $R_k(\theta)$ about an angle θ may be written

$$R_k(\theta) = \exp[-i\theta I_k] \tag{7}$$

where $k = \pm x, \pm y$. The spin operators for $I = 1$, $I = 3/2$ and $I = 5/2$ have rotations in basis of the SU(3), SU(4) and SU(6) Lie Algebra groups, respectively [19]. In the above equations, H_{int} refers to internal Hamiltonian, which for our spin system is given by Eq. (1). When a rotation is made that transforms the system to a toggling frame, the toggling frame quadrupolar Hamiltonian is described by the relationship

$$\widetilde{H}_{int} = U_{RF}^{-1}H_{int}U_{RF} \tag{8}$$

Given the form of H_{int}, the rotations are of the following form

$$\exp[iI_k\theta]II\exp[-iI_k\theta] = II \tag{9}$$

$$\exp(i\theta I_x)I_zI_z\exp(-i\theta I_x) = \frac{1}{2}(I_yI_y + I_zI_z) - \frac{1}{2}(I_yI_y - I_zI_z)\cos(2\theta) - \frac{1}{2}(I_yI_z + I_yI_z)\sin(2\theta) \tag{10}$$

and

$$\exp(i\theta I_y)I_zI_z\exp(-i\theta I_y) = \frac{1}{2}(I_xI_x + I_zI_z) - \frac{1}{2}(I_xI_x - I_zI_z)\cos(2\theta) + \frac{1}{2}(I_xI_z + I_zI_x)\sin(2\theta) \tag{11}$$

We note that the operators that comprise the toggling frame internal Hamiltonian transform exactly the same way independent of the value of I. Therefore the calculation of the Hamiltonian in the toggling frame is the same independent of the value of I, but the results are different in both dimension and magnitude. The calculation of $\overline{H}^0_{int}$ for an x, y cycle is the same for $I = 1, 3/2$ and $5/2$ and is given by

$$\overline{H}^0_{int} = \frac{W}{6\tau}[I_yI_z + I_zI_y - I_xI_y - I_yI_x] \tag{12}$$

In the above expression, I_x, I_y and I_z are unitary matrix representations of the angular momentum operators for spin $I = 1, 3/2$ and $5/2$, $W = \frac{12\alpha\omega_Q}{\pi}$ and 2α is the $\pi/2$ pulse width.

Next we consider the first-order term of the Magnus expansion for the different values of I given by Eq. (6), which we have rewritten as

$$\overline{H}^1_{int} = \frac{-i}{2t_c}[I_1 + I_2 + \cdots] \tag{13}$$

Because $\overline{H}^1_{int}$ consists of commutators, the calculation for $\overline{H}^1_{int}$ for spin $I = 1, 3/2$ and $5/2$ will be different. For the quadrupolar echo sequence shown in Fig. 1, the toggling frame quadrupolar Hamiltonian during each stage is given in Table 1 of reference [20]. For the computation of the first-order term, the expressions that involve the commutator of toggling Hamiltonians from the same time stage all cancel. That is,

$$\iint[\widetilde{H}_j, \widetilde{H}_k]dt_1\,dt_0 = 0 \tag{14}$$

Table 1
Integrated first-order terms of the Magnus expansion for the quadrupolar Hamiltonian for 8 cycles of the quadrupolar echo pulse sequence in Fig. 1 that produce an echo

Pulse 1	Pulse 2	$\overline{H}^0_{\omega_Q}$
x	y	$\frac{W}{6\tau}[I_yI_z + I_zI_y - I_xI_y - I_yI_x]$
x	$-y$	$\frac{W}{6\tau}[I_yI_z + I_zI_y + I_xI_y + I_yI_x]$
$-x$	y	$\frac{W}{6\tau}[-I_yI_z - I_zI_y + I_xI_y + I_yI_x]$
$-x$	$-y$	$\frac{W}{6\tau}[-I_yI_z - I_zI_y - I_xI_y - I_yI_x]$
y	x	$\frac{W}{6\tau}[-I_xI_y - I_yI_x - I_zI_x - I_xI_z]$
y	$-x$	$\frac{W}{6\tau}[I_xI_y + I_yI_x - I_zI_x - I_xI_z]$
$-y$	x	$\frac{W}{6\tau}[I_xI_y + I_yI_x + I_zI_x + I_xI_z]$
$-y$	$-x$	$\frac{W}{6\tau}[-I_xI_y - I_yI_x + I_zI_x + I_xI_z]$

In the table $W = \frac{12\alpha\omega_Q}{\pi}$, ω_Q is the quadrupolar coupling constant and 2α is the $\pi/2$ pulse width.

for $j = k$. The above expression is true for all the domains of integration, including time δ_2 and δ_4, which are time-dependent.

The remaining terms in the sum have been computed as follows

$$I_1 = \int_{\tau-\alpha}^{\tau+\alpha}\int_0^{\tau-\alpha}[\widetilde{H}_2\cdot\widetilde{H}_1 - \widetilde{H}_1\cdot\widetilde{H}_2]\mathrm{d}t_2\,\mathrm{d}t_1 \tag{15}$$

$$I_2 = \int_{\tau+\alpha}^{2\tau-\alpha}\int_0^{\tau-\alpha}[\widetilde{H}_3\cdot\widetilde{H}_1 - \widetilde{H}_1\cdot\widetilde{H}_3]\mathrm{d}t_3\,\mathrm{d}t_1 + \int_{\tau}^{2\tau-\alpha}\int_{\tau-2\alpha}^{\tau}[\widetilde{H}_3\cdot\widetilde{H}_2 - \widetilde{H}_2\cdot\widetilde{H}_3]\mathrm{d}t_3\,\mathrm{d}t_2 \tag{16}$$

$$I_3 = \int_{2\tau-\alpha}^{2\tau+\alpha}\int_0^{\tau-\alpha}[\widetilde{H}_4\cdot\widetilde{H}_1 - \widetilde{H}_1\cdot\widetilde{H}_4]\mathrm{d}t_4\,\mathrm{d}t_1 + \int_{2\tau-\alpha}^{2\tau+\alpha}\int_{\tau-\alpha}^{\tau+\alpha}[\widetilde{H}_4\cdot\widetilde{H}_2 - \widetilde{H}_2\cdot\widetilde{H}_4]\mathrm{d}t_4\,\mathrm{d}t_2 + \int_{2\tau-\alpha}^{2\tau+\alpha}\int_{\tau+\alpha}^{2\tau-\alpha}[\widetilde{H}_4\cdot\widetilde{H}_3 - \widetilde{H}_3\cdot\widetilde{H}_4]\mathrm{d}t_4\,\mathrm{d}t_3 \tag{17}$$

$$I_4 = \int_{2\tau+\alpha}^{3\tau}\int_0^{\tau-\alpha}[\widetilde{H}_5\cdot\widetilde{H}_1 - \widetilde{H}_1\cdot\widetilde{H}_5]\mathrm{d}t_5\,\mathrm{d}t_1 + \int_{2\tau+\alpha}^{3\tau}\int_{\tau-\alpha}^{\tau+\alpha}[\widetilde{H}_5\cdot\widetilde{H}_2 - \widetilde{H}_2\cdot\widetilde{H}_5]\mathrm{d}t_5\,\mathrm{d}t_2 + \int_{2\tau+\alpha}^{3\tau}\int_{\tau+\alpha}^{2\tau-\alpha}[\widetilde{H}_5\cdot\widetilde{H}_3 - \widetilde{H}_3\cdot\widetilde{H}_5]\mathrm{d}t_5\,\mathrm{d}t_3 + \int_{2\tau+\alpha}^{3\tau}\int_{2\tau-\alpha}^{2\tau+\alpha}[\widetilde{H}_5\cdot\widetilde{H}_4 - \widetilde{H}_4\cdot\widetilde{H}_5]\mathrm{d}t_5\,\mathrm{d}t_4 \tag{18}$$

From the above expressions, it is evident that the first-order term of the Magnus expansion may consist of terms that are contributions from double integrals involving delay terms multiplying pulse terms, pulse terms multiplying pulse terms or delay terms multiplying delay terms.

For spin $I = 1$ we find,

$$I_1 = \frac{-18\mathrm{i}\alpha^2\omega_Q^2\sin\left[\frac{\pi(\alpha-\tau)}{4\alpha}\right]^2}{4\pi}I_x \tag{19}$$

$$I_2 = \frac{-18\mathrm{i}\alpha^2\omega_Q^2\cos\left[\frac{\pi\tau}{4\alpha}\right]^2}{4\pi}I_x \tag{20}$$

$$I_3 = \left[\frac{18\mathrm{i}\alpha^2\omega_Q^2\cos\left[\frac{\pi\tau}{4\alpha}\right]^2}{4\pi} - \frac{18\mathrm{i}\alpha^2\omega_Q^2\left[\pi\cos\left(\frac{\pi\tau}{2\alpha}\right)+\sin\left(\frac{\pi\tau}{\alpha}\right)\right]}{8\pi^2}\right]I_z + \frac{18\mathrm{i}\alpha^2\omega_Q^2\left[1+\cos\left(\frac{\pi\tau}{\alpha}\right)\right]}{8\pi^2}I_y + \frac{18\mathrm{i}h\alpha^2\omega_Q^2\left[\pi\cos\left(\frac{\pi\tau}{2\alpha}\right)+\sin\left(\frac{\pi\tau}{\alpha}\right)\right]}{8\pi^2}I_x \tag{21}$$

$$I_4 = \frac{18\mathrm{i}\alpha^2\omega_Q^2\cos\left[\frac{\pi(\alpha+\tau)}{4\alpha}\right]^2}{4\pi}I_z \tag{22}$$

Summing up all four terms of the integral, the first-order term of the Magnus expansion for an x, y quadrupolar echo cycle for spin $I = 1$ reduces to

$$\overline{H}^1_{\mathrm{int}} = \frac{B}{6\tau}I_y - \frac{A}{6\tau}I_z + \frac{A}{6\tau}I_x \tag{23}$$

where

$$A = \frac{18\alpha^2\omega_Q^2\left[\pi(-2+\sin\left(\frac{\pi\tau}{2\alpha}\right))+\sin\left(\frac{\pi\tau}{\alpha}\right)\right]}{\pi^2} \tag{24}$$

and

$$B = \frac{18\alpha^2\omega_Q^2\left[1+\cos\left(\frac{\pi\tau}{\alpha}\right)\right]}{\pi^2} \tag{25}$$

Together with Eq. (14), these results indicate that the only terms that remain are terms that are quadratic in α. As a consequence, all the higher order terms are expected to vanish in the case that the pulse width approaches zero.

For spin-3/2 and 5/2, we have taken $\alpha \ll \tau$, so that terms quadratic in α^2 are neglected. This assumption makes physical sense as the pulse width, 2α, is usually on the order of 1 μs while the pulse spacing time, τ, is typically on the order of 10–100 μs. Working out all the terms (I_1, I_2, I_3, I_4) for spin $I = 3/2$ and 5/2, the first-order term of the Magnus expansion for an x, y quadrupolar echo cycle was computed. For the case of $I = 3/2$, we find

$$\overline{H}^1_{\mathrm{int}} = \frac{-\mathrm{i}}{6\tau}\begin{pmatrix} 0 & 0 & 9\sqrt{3}\tau^2\omega_Q^2 & 0 \\ 0 & 0 & 0 & -9\sqrt{3}\tau^2\omega_Q^2 \\ -9\sqrt{3}\tau^2\omega_Q^2 & 0 & 0 & 0 \\ 0 & 9\sqrt{3}\tau^2\omega_Q^2 & 0 & 0 \end{pmatrix} \tag{26}$$

For the case $I = 5/2$, we find

$$\overline{H}^1_{\mathrm{int}} = \frac{-\mathrm{i}}{6\tau}\begin{pmatrix} 0 & 0 & 27\sqrt{10}\tau^2\omega_Q^2 & 0 & 0 & 0 \\ 0 & 0 & 0 & 27\sqrt{2}\tau^2\omega_Q^2 & 0 & 0 \\ -27\sqrt{10}\tau^2\omega_Q^2 & 0 & 0 & 0 & -27\sqrt{2}\tau^2\omega_Q^2 & 0 \\ 0 & -27\sqrt{10}\tau^2\omega_Q^2 & 0 & 0 & 0 & -27\sqrt{10}\tau^2\omega_Q^2 \\ 0 & 0 & 27\sqrt{2}\tau^2\omega_Q^2 & 0 & 0 & 0 \\ 0 & 0 & 0 & 27\sqrt{10}\tau^2\omega_Q^2 & 0 & 0 \end{pmatrix} \tag{27}$$

In contrast to the results obtained for spin $I = 1$, the above results indicate a contributing factor that scales as τ^2. This term arises from the non-zero commutator of delay terms times delay terms in the first-order term of the Magnus expansion. As a consequence of this result, even for delta function RF pulses, the first-order term and all higher order terms are non-zero.

With the above results, we study the range of validity of AHT by comparing this perturbation approach to a numerical solution of the VN equation. The analysis is based on comparing the single and multiple quantum coherences in the density matrix at 3τ for the solution obtained by AHT to that obtained by the VN equation.

By using the $\rho_{AHT}(3\tau)$ and $\rho_{VN}(3\tau)$, we compute the single quantum (SQ) and double quantum (DQ) coherences of the density matrix. Fig. 2A highlights the absolute value of the difference of these two values as a function of ω_Q for different values of τ. For quadrupolar frequencies below 250 kHz, a pulse width of 2α=1 μs and pulse spacings as large as τ=25 μs, first-order AHT appears to come within 80 percent of the solution predicted by the numerical calculation from the VN equation for $I = 1$. However, the situation is more complex for the multiple quantum coherences. Fig. 2B highlights the difference of DQ coherences computed from first-order AHT to that of the DQ coherences from a numerical solution of the VN equation at 3τ. The results show that AHT predicts these coherences only in the case of short pulse spacings and much weaker coupling. A similar analysis was extended to the case of $I = 3/2$ and $I = 5/2$. Figs. 3A and 4A again highlight the difference of SQ coherences at 3τ as predicted by AHT and a numerical solution of the VN equation for $I = 3/2$ and $I = 5/2$ respectively. Figs. 3B and 4B show the difference of TQ coherences at 3τ as predicted by AHT and a numerical solution of the VN equation for $I = 3/2$ and $I = 5/2$ respectively. The results indicate that the dynamics appear more complex for these higher spin systems for the range of τ and ω_q studied. Whereas AHT appears to predict the dynamics quite well for spin $I = 1$ over a large bandwidth, the perturbation scheme works well only for small τ spacings and small bandwidths for $I = 3/2$ and $I = 5/2$ as expected from the analysis presented above.

The size of the zero-order term relative to the first-order term contribution for $I = 3/2$ and $5/2$ should be emphasized. In the case of spin $I = 1$, we found that the first-order term is proportional to α^2. On the other hand, the first-order term for spin $I = 3/2$ and $I = 5/2$ included a τ^2 dependence. Thus for spin $I = 3/2$ and $I = 5/2$ systems, the zero-order contribution is only relevant if the first-order contribution does not dominate, i.e. for small τ. Referring to Figs. 3 and 4, the agreement for the SQ coherences between AHT and the VN equation is good over a bandwidth of approximately 50 kHz, when $\tau = 2$ μs for both $I = 3/2$ and $I = 5/2$. For a larger pulse spacing of $\tau = 10$ μs, the agreement is shown to deteriorate. In contrast, Fig. 2 indicates that the agreement between SQ coherences computed by AHT and the VN equation for spin $I = 1$ is relatively independent of the pulse spacing. However, the situation is more complex for the higher order coherences. Referring to Fig. 2B for $I = 1$, the agreement between DQ coherences computed by AHT and the VN equation appears tau dependent. A similar finding was observed for the TQ coherences for spin $I = 3/2$ and $I = 5/2$ shown in Figs. 3 and 4. This is likely due to higher order terms of the Magnus expansion that have not been included in our calculation. As higher order terms are accounted for in the system dynamics, however, it is expected that AHT should converge to a numerical solution obtained by the VN equation. As a further test of the contribution of the first-order term of the Magnus expansion to the system dynamics, we consider the same pulse sequence and compare the results in the case when only the zeroth-order term is accounted for, and then when the first-order term is taken into account. Fig. 5 highlights the difference of SQ coherences as predicted by AHT to a numerical solution of the VN equation to zeroth $(H^1_{\omega_q} = 0)$ and then to first-order $(H^1_{\omega_q} \neq 0)$ for the case of spin $I = 1$. The results show that for two different values of τ that the first-order term contributes little to the dynamics. Figs. 6 and 7 highlight a similar calculation for $I = 3/2$ and $5/2$ respectively. In each case, the dynamics as predicted by AHT appear to be in better agreement when the first-order term is accounted for, especially for these cases. Thus it is expected that as higher order terms are taken into account, AHT is expected to converge to the solution obtained by the VN equation.

Next we focus on the effects of finite pulse widths on the spectra of spin $I = 1$, $3/2$ and $5/2$ nuclei acquired by the pulse sequence shown in Fig. 1. The analysis presented above will be used in a simple test to probe our ability to predict the spin dynamics based on zeroth order AHT. In a previous paper, we reported on a phase cycling scheme that suppresses artifacts for spin $I = 1$ nuclei for the

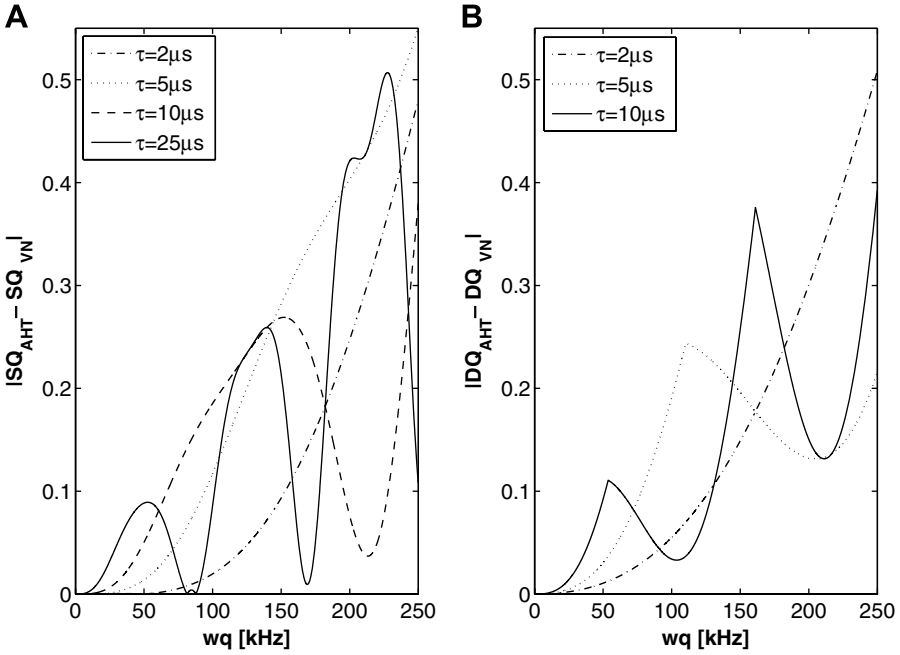

Fig. 2. (A) Absolute value of the difference of the observable single quantum (SQ) coherences for $I = 1$ as predicted by first-order AHT and that from a numerical solution to the VN equation for the pulse sequence shown in Fig. 1 for different values of τ. (B) Absolute value of the difference of the double quantum (DQ) coherences for $I = 1$ as predicted by first-order AHT and that from a numerical solution to the VN equation for the same pulse sequence and different values of τ. In both simulations, the $\pi/2$ pulse width was taken to be 1 μs.

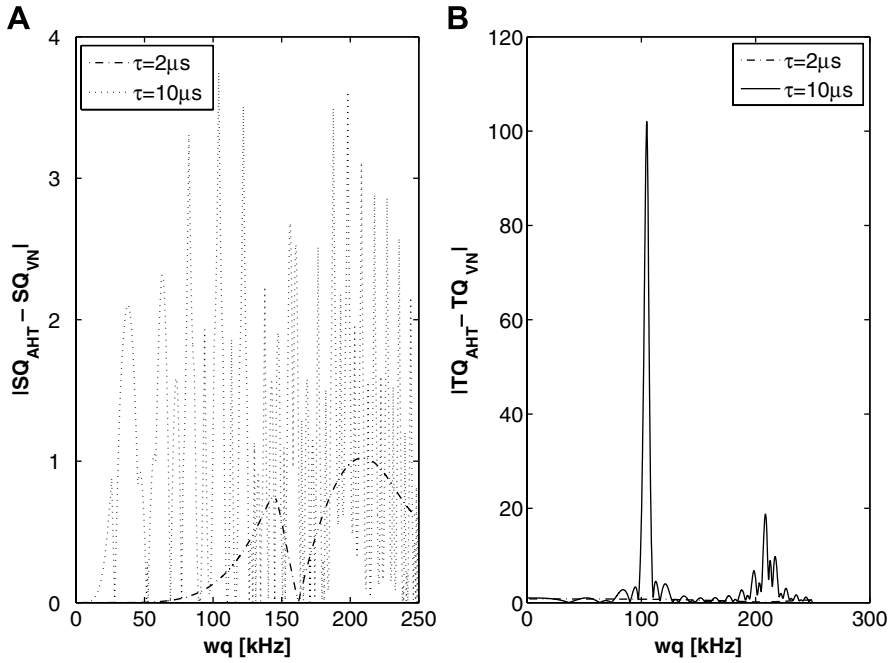

Fig. 3. (A) Absolute value of the difference of the observable single quantum (SQ) coherences for $I = 3/2$ as predicted by first-order AHT and that from a numerical solution to the VN equation for the pulse sequence shown in Fig. 1 for different values of τ. (B) Absolute value of the difference of the triple quantum (TQ)coherences for $I = 3/2$ as predicted by first-order AHT and that from a numerical solution to the VN equation for the same pulse sequence and different values of τ. In both simulations, the $\pi/2$ pulse width was taken to be 1 μs.

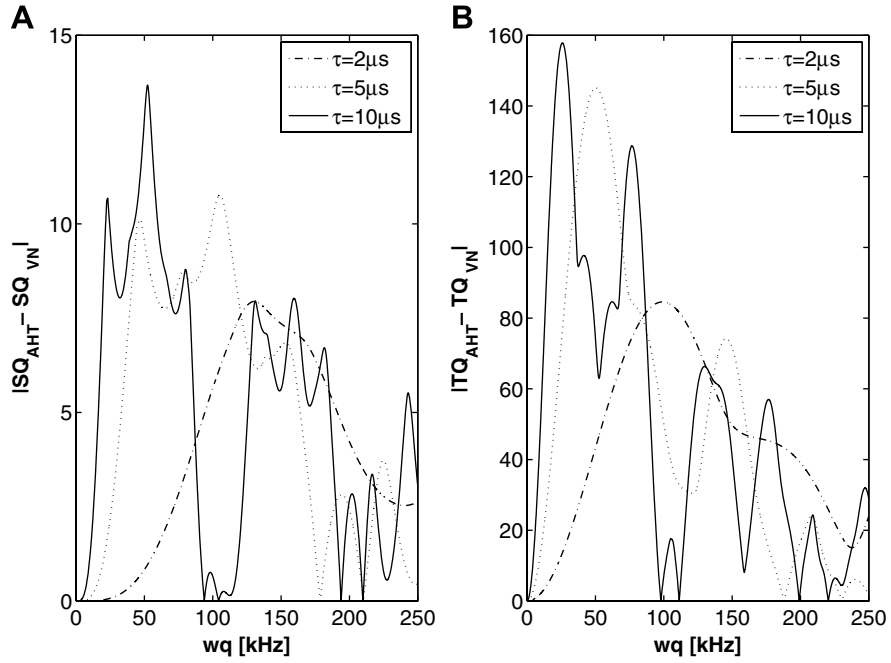

Fig. 4. (A) Absolute value of the difference of the observable single quantum (SQ) coherences for $I = 5/2$ as predicted by first-order average Hamiltonian theory and that from a numerical solution to the VN equation for the pulse sequence shown in Fig. 1 for different values of τ. (B) Absolute value of the difference of the triple quantum coherence for $I = 5/2$ as predicted by first-order AHT and that from a numerical solution to the VN equation for the same pulse sequence and different values of τ. In both simulations, the $\pi/2$ pulse width was taken to be 1 μs.

same quadrupolar echo sequence shown in Fig. 1 [20]. In that work, a spectral artifact was shown to arise from the compound evolution of the spin system evolving under both the RF and quadrupolar Hamiltonian during the pulses delivered to the spin system resulting in an asymmetric quadrupolar pattern. By cycling the phases of the RF pulses and receiver in a well-defined manner, it was shown that this artifact may be suppressed to zeroth-order of the Magnus expansion. To verify the calculations presented above, we implement the same phase cycling scheme on spin $I = 3/2$ and $I = 5/2$ nuclei and then test these cycles experimentally and by simulation.

Given the density matrix of the spin system at time 3τ, the state of the system at any point in time t_k is given by

$$\rho_{\mathrm{AHT,VN}}(t_k) = \exp(-\mathrm{i}H_Q t_k)\rho(3\tau)_{\mathrm{AHT,VN}} \exp(\mathrm{i}H_Q t_k) \tag{28}$$

where H_Q is given in Eq. (1). The detected signal at time t_k is found by performing the computation

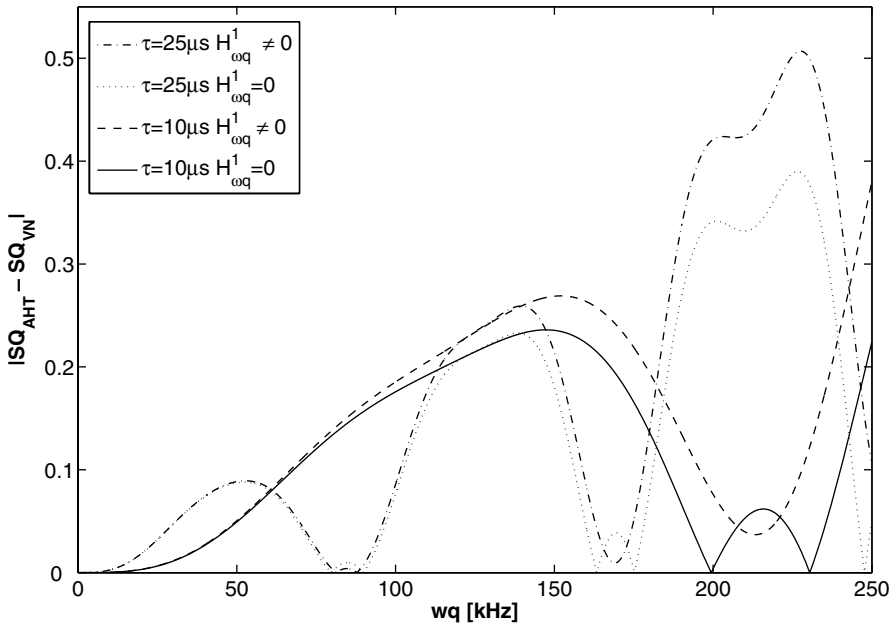

Fig. 5. Absolute value of the difference of the observable single quantum (SQ) coherences for $I = 1$ as predicted by first-order AHT and that from a numerical solution to the VN equation for the pulse sequence shown in Fig. 1 for two different values of τ. The figure highlights the differences when only the first term in the Magnus expansion is taken (i.e. $H^1_{\omega q} = 0$) and the improvement when the second term in the Magnus expansion is accounted for (i.e. $H^1_{\omega q} \neq 0$).

$$\text{Signal}(t_k) = \text{Trace}\{\rho(t_k)[I_x + \mathrm{i}I_y]\} \tag{29}$$

For an x, y cycle, according to the VN equation, the state of the spin system at 3τ is given by

$$\begin{aligned}\rho(3\tau)_{\text{VN}} = {} & \exp[-\mathrm{i}H_Q(\tau-\alpha)]\exp[-\mathrm{i}\omega_{rf}I_y 2\alpha + \mathrm{i}H_Q 2\alpha] \\ & \exp[-\mathrm{i}H_Q(\tau-2\alpha)]\exp[-\mathrm{i}\omega_{rf}I_x 2\alpha - \mathrm{i}H_Q 2\alpha]\rho(0) \\ & \exp[\mathrm{i}\omega_{rf}I_x 2\alpha + \mathrm{i}H_Q 2\alpha]\exp[\mathrm{i}H_Q(\tau-2\alpha)] \\ & \exp[\mathrm{i}\omega_{rf}I_y 2\alpha - \mathrm{i}H_Q 2\alpha]\exp[\mathrm{i}H_Q(\tau-\alpha)]\end{aligned} \tag{30}$$

By AHT, the density matrix at 3τ is given by Eq. (3). In the following, we only consider the zeroth-order term of the Magnus expansion in our simulations. By evolving $\rho(3\tau)_{\text{AHT, VN}} \rightarrow \rho(3\tau + t)_{\text{AHT,VN}}$ under Eq. (1), we simulated the spectra of powdered sample of spin $I = 1$, 3/2 and 5/2.

2.1. Spin-3/2

Taking the results for the first-order term of the Magnus expansion given in Table 1 and Eq. (4), the density matrices at 3τ, $\rho(3\tau)$, for all eight cycles of the quadrupolar echo pulse sequence for a spin system of $I = 3/2$ nuclei are provided below. Each density matrix highlights the effect of finite pulse widths on the system evolution and the state of the system at 3τ.

$$\rho^{\text{AHT}}_{x,y}(3\tau) = \begin{pmatrix} -A_{11} - \frac{\sqrt{6}}{2}A_{12} & -\mathrm{i}\left(\frac{\sqrt{3}}{2}A_{13} + \frac{\sqrt{2}}{2}A_{12}\right) & -\frac{\sqrt{3}}{2}A_{11} + \frac{\sqrt{2}}{2}A_{12} & 0 \\ \mathrm{i}\left(\frac{\sqrt{3}}{2}A_{13} + \frac{\sqrt{2}}{2}A_{12}\right) & \frac{\sqrt{6}}{2}A_{12} & -\mathrm{i}A_{13} & \frac{\sqrt{3}}{2}A_{11} + \frac{\sqrt{2}}{2}A_{12} \\ -\frac{\sqrt{3}}{2}A_{11} + \frac{\sqrt{2}}{2}A_{12} & \mathrm{i}A_{13} & \frac{\sqrt{6}}{2}A_{12} & -\mathrm{i}\left(\frac{\sqrt{3}}{2}A_{13} - \frac{\sqrt{2}}{2}A_{12}\right) \\ 0 & \frac{\sqrt{3}}{2}A_{11} + \frac{\sqrt{2}}{2}A_{12} & \mathrm{i}\left(\frac{\sqrt{3}}{2}A_{13} - \frac{\sqrt{2}}{2}A_{12}\right) & A_{11} - \frac{\sqrt{6}}{2}A_{12} \end{pmatrix} \tag{31}$$

$$\rho^{\text{AHT}}_{x,-y}(3\tau) = \begin{pmatrix} -A_{11} + \frac{\sqrt{6}}{2}A_{12} & -\mathrm{i}\left(\frac{\sqrt{3}}{2}A_{13} - \frac{\sqrt{2}}{2}A_{12}\right) & -\frac{\sqrt{3}}{2}A_{11} - \frac{\sqrt{2}}{2}A_{12} & 0 \\ \mathrm{i}\left(\frac{\sqrt{3}}{2}A_{13} - \frac{\sqrt{2}}{2}A_{12}\right) & -\frac{\sqrt{6}}{2}A_{12} & -\mathrm{i}A_{13} & \frac{\sqrt{3}}{2}A_{11} - \frac{\sqrt{2}}{2}A_{12} \\ -\frac{\sqrt{3}}{2}A_{11} - \frac{\sqrt{2}}{2}A_{12} & \mathrm{i}A_{13} & -\frac{\sqrt{6}}{2}A_{12} & -\mathrm{i}\left(\frac{\sqrt{3}}{2}A_{13} + \frac{\sqrt{2}}{2}A_{12}\right) \\ 0 & \frac{\sqrt{3}}{2}A_{11} - \frac{\sqrt{2}}{2}A_{12} & \mathrm{i}\left(\frac{\sqrt{3}}{2}A_{13} + \frac{\sqrt{2}}{2}A_{12}\right) & A_{11} + \frac{\sqrt{6}}{2}A_{12} \end{pmatrix} \tag{32}$$

$$\rho^{\text{AHT}}_{-x,y}(3\tau) = \begin{pmatrix} -A_{11} + \frac{\sqrt{6}}{2}A_{12} & \mathrm{i}\left(\frac{\sqrt{3}}{2}A_{13} - \frac{\sqrt{2}}{2}A_{12}\right) & -\frac{\sqrt{3}}{2}A_{11} - \frac{\sqrt{2}}{2}A_{12} & 0 \\ -\mathrm{i}\left(\frac{\sqrt{3}}{2}A_{13} - \frac{\sqrt{2}}{2}A_{12}\right) & -\frac{\sqrt{6}}{2}A_{12} & \mathrm{i}A_{13} & \frac{\sqrt{3}}{2}A_{11} - \frac{\sqrt{2}}{2}A_{12} \\ -\frac{\sqrt{3}}{2}A_{11} - \frac{\sqrt{2}}{2}A_{12} & -\mathrm{i}A_{13} & -\frac{\sqrt{6}}{2}A_{12} & \mathrm{i}\left(\frac{\sqrt{3}}{2}A_{13} + \frac{\sqrt{2}}{2}A_{12}\right) \\ 0 & \frac{\sqrt{3}}{2}A_{11} - \frac{\sqrt{2}}{2}A_{12} & -\mathrm{i}\left(\frac{\sqrt{3}}{2}A_{13} + \frac{\sqrt{2}}{2}A_{12}\right) & A_{11} + \frac{\sqrt{6}}{2}A_{12} \end{pmatrix} \tag{33}$$

$$\rho^{\text{AHT}}_{-x,-y}(3\tau) = \begin{pmatrix} -A_{11} - \frac{\sqrt{6}}{2}A_{12} & \mathrm{i}\left(\frac{\sqrt{3}}{2}A_{13} + \frac{\sqrt{2}}{2}A_{12}\right) & -\frac{\sqrt{3}}{2}A_{11} + \frac{\sqrt{2}}{2}A_{12} & 0 \\ -\mathrm{i}\left(\frac{\sqrt{3}}{2}A_{13} + \frac{\sqrt{2}}{2}A_{12}\right) & \frac{\sqrt{6}}{2}A_{12} & \mathrm{i}A_{13} & \frac{\sqrt{3}}{2}A_{11} + \frac{\sqrt{2}}{2}A_{12} \\ -\frac{\sqrt{3}}{2}A_{11} + \frac{\sqrt{2}}{2}A_{12} & -\mathrm{i}A_{13} & \frac{\sqrt{6}}{2}A_{12} & \mathrm{i}\left(\frac{\sqrt{3}}{2}A_{13} - \frac{\sqrt{2}}{2}A_{12}\right) \\ 0 & \frac{\sqrt{3}}{2}A_{11} + \frac{\sqrt{2}}{2}A_{12} & -\mathrm{i}\left(\frac{\sqrt{3}}{2}A_{13} - \frac{\sqrt{2}}{2}A_{12}\right) & A_{11} - \frac{\sqrt{6}}{2}A_{12} \end{pmatrix} \tag{34}$$

$$\rho^{\mathrm{AHT}}_{y,x}(3\tau)=\begin{pmatrix} -A_{11}+\frac{\sqrt{6}}{2}A_{12} & -\frac{\sqrt{3}}{2}A_{13}+\frac{\sqrt{2}}{2}A_{12} & \frac{\sqrt{3}}{2}A_{11}+\frac{\sqrt{2}}{2}A_{12} & 0\\ -\frac{\sqrt{3}}{2}A_{13}+\frac{\sqrt{2}}{2}A_{12} & -\frac{\sqrt{6}}{2}A_{12} & -A_{13} & -\frac{\sqrt{3}}{2}A_{11}+\frac{\sqrt{2}}{2}A_{12}\\ \frac{\sqrt{3}}{2}A_{11}+\frac{\sqrt{2}}{2}A_{12} & -A_{13} & -\frac{\sqrt{6}}{2}A_{12} & -\frac{\sqrt{3}}{2}A_{13}-\frac{\sqrt{2}}{2}A_{12}\\ 0 & -\frac{\sqrt{3}}{2}A_{11}+\frac{\sqrt{2}}{2}A_{12} & -\frac{\sqrt{3}}{2}A_{13}-\frac{\sqrt{2}}{2}A_{12} & A_{11}+\frac{\sqrt{6}}{2}A_{12}\end{pmatrix} \tag{35}$$

$$\rho^{\mathrm{AHT}}_{y,-x}(3\tau)=\begin{pmatrix} -A_{11}-\frac{\sqrt{6}}{2}A_{12} & -\frac{\sqrt{3}}{2}A_{13}-\frac{\sqrt{2}}{2}A_{12} & \frac{\sqrt{3}}{2}A_{11}-\frac{\sqrt{2}}{2}A_{12} & 0\\ -\frac{\sqrt{3}}{2}A_{13}-\frac{\sqrt{2}}{2}A_{12} & \frac{\sqrt{6}}{2}A_{12} & -A_{13} & -\frac{\sqrt{3}}{2}A_{11}-\frac{\sqrt{2}}{2}A_{12}\\ \frac{\sqrt{3}}{2}A_{11}-\frac{\sqrt{2}}{2}A_{12} & -A_{13} & \frac{\sqrt{6}}{2}A_{12} & -\frac{\sqrt{3}}{2}A_{13}+\frac{\sqrt{2}}{2}A_{12}\\ 0 & -\frac{\sqrt{3}}{2}A_{11}-\frac{\sqrt{2}}{2}A_{12} & -\frac{\sqrt{3}}{2}A_{13}+\frac{\sqrt{2}}{2}A_{12} & A_{11}-\frac{\sqrt{6}}{2}A_{12}\end{pmatrix} \tag{36}$$

$$\rho^{\mathrm{AHT}}_{-y,x}(3\tau)=\begin{pmatrix} -A_{11}-\frac{\sqrt{6}}{2}A_{12} & \frac{\sqrt{3}}{2}A_{13}+\frac{\sqrt{2}}{2}A_{12} & \frac{\sqrt{3}}{2}A_{11}-\frac{\sqrt{2}}{2}A_{12} & 0\\ \frac{\sqrt{3}}{2}A_{13}+\frac{\sqrt{2}}{2}A_{12} & \frac{\sqrt{6}}{2}A_{12} & A_{13} & -\frac{\sqrt{3}}{2}A_{11}-\frac{\sqrt{2}}{2}A_{12}\\ \frac{\sqrt{3}}{2}A_{11}-\frac{\sqrt{2}}{2}A_{12} & A_{13} & \frac{\sqrt{6}}{2}A_{12} & \frac{\sqrt{3}}{2}A_{13}-\frac{\sqrt{2}}{2}A_{12}\\ 0 & -\frac{\sqrt{3}}{2}A_{11}-\frac{\sqrt{2}}{2}A_{12} & \frac{\sqrt{3}}{2}A_{13}-\frac{\sqrt{2}}{2}A_{12} & A_{11}-\frac{\sqrt{6}}{2}A_{12}\end{pmatrix} \tag{37}$$

$$\rho^{\mathrm{AHT}}_{-y,-x}(3\tau)=\begin{pmatrix} -A_{11}+\frac{\sqrt{6}}{2}A_{12} & \frac{\sqrt{3}}{2}A_{13}-\frac{\sqrt{2}}{2}A_{12} & \frac{\sqrt{3}}{2}A_{11}+\frac{\sqrt{2}}{2}A_{12} & 0\\ \frac{\sqrt{3}}{2}A_{13}-\frac{\sqrt{2}}{2}A_{12} & -\frac{\sqrt{6}}{2}A_{12} & A_{13} & -\frac{\sqrt{3}}{2}A_{11}+\frac{\sqrt{2}}{2}A_{12}\\ \frac{\sqrt{3}}{2}A_{11}+\frac{\sqrt{2}}{2}A_{12} & A_{13} & -\frac{\sqrt{6}}{2}A_{12} & \frac{\sqrt{3}}{2}A_{13}+\frac{\sqrt{2}}{2}A_{12}\\ 0 & -\frac{\sqrt{3}}{2}A_{11}+\frac{\sqrt{2}}{2}A_{12} & \frac{\sqrt{3}}{2}A_{13}+\frac{\sqrt{2}}{2}A_{12} & A_{11}+\frac{\sqrt{6}}{2}A_{12}\end{pmatrix} \tag{38}$$

In the above expressions, the constants A_{11}, A_{12} and A_{13} are given by the relations

$$\begin{aligned} A_{11}&=1-\cos\left(\sqrt{6}W\right)\\ A_{12}&=\sin\left(\sqrt{6}W\right)\\ A_{13}&=1+\cos\left(\sqrt{6}W\right)\end{aligned} \tag{39}$$

The constant W is again given by

$$W=\frac{12\alpha\omega_{\mathrm{Q}}}{\pi} \tag{40}$$

where 2α is the $\pi/2$ pulse width. Consider the case of a $\frac{\pi}{2}$ pulse about the x-axis followed by a $\frac{\pi}{2}$ pulse about the y-axis. In the limit of delta function RF pulses ($\alpha\to 0$), the constant W will be zero, and the constants A_{11} and A_{12} will be zero. In this idealized limit, the DQ coherences vanish, and one is left with only SQ coherences. However, with even modest RF pulse power, α can only be made on the order of 1 μs, and so the system at the echo peak will also contain a DQ coherence. This double coherence does not evolve to SQ coherences under the secular quadrupolar interaction given in Eq. (1) and is not detectable. However, the SQ coherences for any given cycle above is the combination of both even and odd functions. For instance, in the case of an x, y cycle, the sum of A_{13} and A_{12} is the sum of even and odd functions. Upon performing a Fourier transform of the signal from the echo peak, the sum of odd and even functions will result in an asymmetric spectrum. The artifact cannot be corrected by phasing the spectra due to the presence of both odd and even functions in the signal.

With the goal of canceling this artifact in the detected signal, we wish to remove the odd and even functions that comprise the SQ coherences of the density matrix at 3τ. For spin $I=1$, we found one such phase cycle is given by the following phase cycling scheme

$$\begin{aligned} \phi_1&=\{x,x,-x,-x,y,y,-y,-y\}\\ \phi_2&=\{y,-y,y,-y,x,-x,x,-x\}\\ \mathrm{RP}&=\{270,270,90,90,0,0,180,180\}\end{aligned} \tag{41}$$

where ϕ_1 is the phase of the first pulse, ϕ_2 is the phase of the second pulse and RP is the receiver phase and is given in degrees [20].

Using the above results, the signal detected is given by

$$\begin{aligned} \mathrm{Signal}(3\tau)^{\mathrm{AHT}}=\mathrm{Trace}\Big\{&\left(\rho^{\mathrm{AHT}}_{x,y}(3\tau)\right)+\rho^{\mathrm{AHT}}_{x,-y}(3\tau)\\ &-\left(\rho^{\mathrm{AHT}}_{-x,y}(3\tau)-\rho^{\mathrm{AHT}}_{-x,-y}(3\tau)\right)\left(-I_{y,1}+\mathrm{i}I_{x,1}\right)\\ &\times\left(\rho^{\mathrm{AHT}}_{y,x}(3\tau)+\rho^{\mathrm{AHT}}_{y,-x}(3\tau)-\rho^{\mathrm{AHT}}_{-y,x}(3\tau)-\rho^{\mathrm{AHT}}_{-y,-x}(3\tau)\right)\\ &\times\left(I_{x,1}+\mathrm{i}I_{y,1}\right)\Big\}\end{aligned} \tag{42}$$

and reduces to the following expression

$$\mathrm{Signal}(3\tau)^{\mathrm{AHT}}=2\left(1+\cos\left(\sqrt{6}W\right)\right)\left\{I_y(-I_y+\mathrm{i}I_x)-I_x(I_x+\mathrm{i}I_y)\right\} \tag{43}$$

with $W=\frac{12\alpha\omega_{\mathrm{Q}}}{\pi}$. The amplitude modulation, $2\left(1+\cos\left(\sqrt{6}W\right)\right)$, reduces the signal intensity symmetrically over the spectrum and will depend on the width of the $\pi/2$ pulses.

Fig. 8 highlights simulated spectra for spin $I=3/2$ by using a dwell time equal to 0.25 μs and a quadrupolar coupling constant equal to 80 kHz. We assumed a sample with a random distribution of orientations, a quadrupolar asymmetry parameter $\eta=0$, set the pulse width 2α to 1 μs and $\tau=50$ μs. The results shown in Fig. 8A show the case of a cycle where the first pulse was $\pi/2$ about the x-axis, and the second pulse was $\pi/2$ about the y-axis. The spectra appear distorted and asymmetric. Fig. 8B highlights the result when the signals are co-added using the phase cycling scheme suggested in Eq. (41), and the distortion is removed to some extent resulting in symmetric spectra. The simulation results should be contrasted to the experimental data shown in Fig. 9, which are discussed in Section 3.

2.2. Spin I = 5/2

Using Eq. (3). and the zeroth-order terms of the Magnus expansion, the density matrices at 3τ for all eight cycles of the quadrupolar echo pulse sequence were computed for spin $I=5/2$ and are given in matrix form below

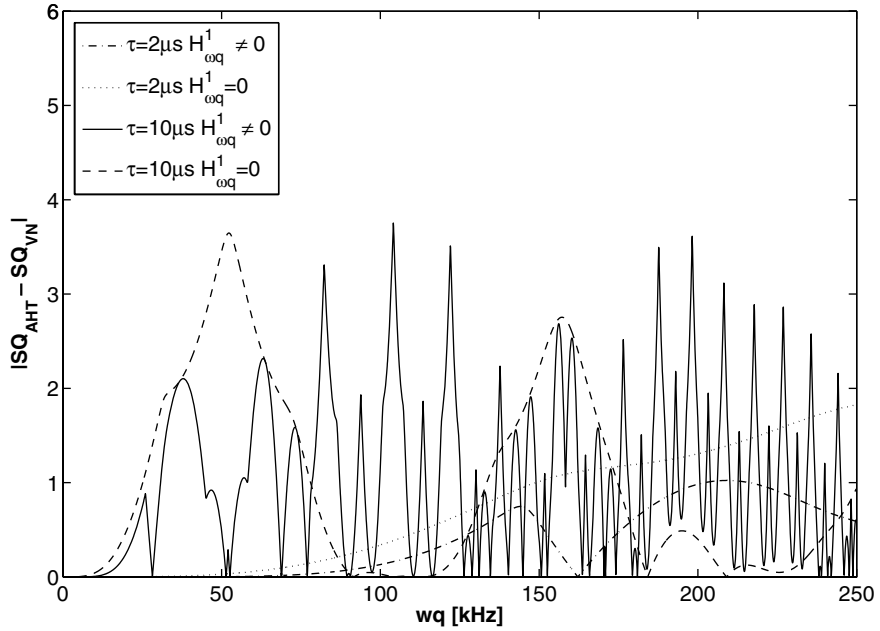

Fig. 6. Absolute value of the difference of the observable single quantum coherence (SQ) for $I = 3/2$ as predicted by first-order AHT and that from a numerical solution to the VN equation for the pulse sequence shown in Fig. 1 for two different values of τ. The figure highlights the differences when only the first term in the Magnus expansion is taken (i.e. $H^1_{\omega q} = 0$) and the improvement when the second term in the Magnus expansion is accounted for (i.e. $H^1_{\omega q} \neq 0$).

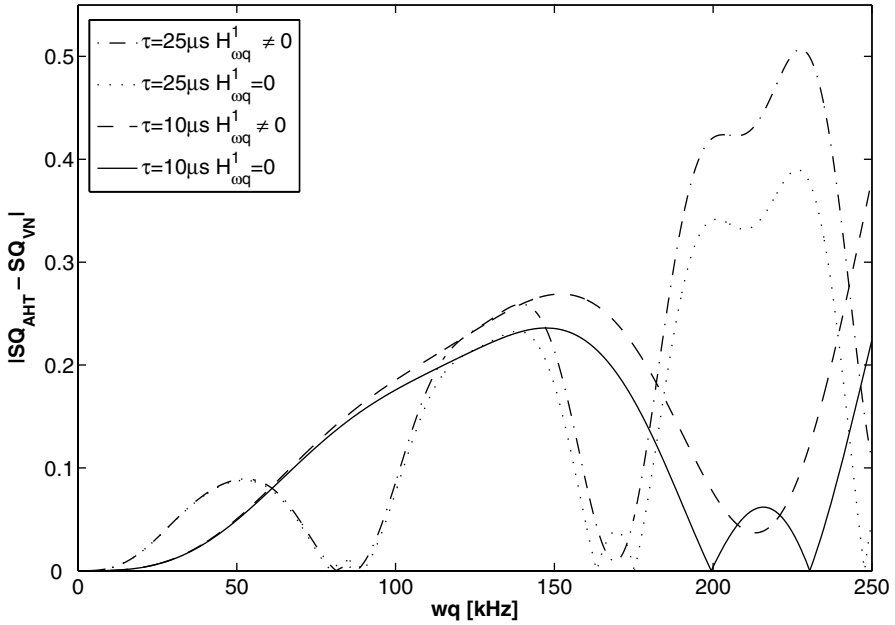

Fig. 7. Absolute value of the difference of the observable single quantum (SQ) coherences for $I = 5/2$ as predicted by first-order AHT and that from a numerical solution to the VN equation for the pulse sequence shown in Fig. 1 for two different values of τ. The figure highlights the differences when only the first term in the Magnus expansion is taken (i.e. $H^1_{\omega q} = 0$) and the improvement when the second term in the Magnus expansion is accounted for (i.e. $H^1_{\omega q} \neq 0$).

$$\rho^{\mathrm{AHT}}_{x,y}(3\tau) = \begin{pmatrix} A_{25} - A_{26} & -\mathrm{i}\left(A_{27} + \frac{A_{21}}{4}\right) & A_{28} & -\mathrm{i}\left(A_{29} - \frac{A_{22}}{4}\right) & -\sqrt{2}(2A_{29} + \frac{A_{22}}{8}) & -\mathrm{i}\frac{5}{8}\sqrt{10}A_{22} \\ \mathrm{i}\left(A_{27} + \frac{A_{21}}{4}\right) & A_{211} + A_{212} & -\mathrm{i}\left(A_{210} + \frac{A_{23}}{4}\right) & A_{213} - A_{214} & -\mathrm{i}\frac{7}{8}\sqrt{10}A_{22} & -\sqrt{2}(2A_{29} - \frac{A_{22}}{8}) \\ A_{28} & \mathrm{i}\left(A_{210} + \frac{A_{23}}{4}\right) & A_{215} + \frac{\sqrt{10}}{12}A_{22} & \mathrm{i}\frac{A_{24}}{4} & A_{213} + A_{214} & \mathrm{i}\left(A_{29} + \frac{A_{22}}{4}\right) \\ -\mathrm{i}\left(-A_{29} + \frac{A_{22}}{4}\right) & A_{213} - A_{214} & -\mathrm{i}\frac{A_{24}}{4} & A_{215} - \frac{\sqrt{10}}{12}A_{22} & -\mathrm{i}\left(-A_{210} + \frac{A_{23}}{4}\right) & A_{216} \\ -\sqrt{2}(2A_{29} + \frac{A_{22}}{8}) & \mathrm{i}\frac{49}{56}\sqrt{10}A_{22} & A_{213} + A_{214} & \mathrm{i}\left(-A_{210} + \frac{A_{23}}{4}\right) & A_{212} - A_{211} & \mathrm{i}\left(A_{27} - \frac{A_{21}}{4}\right) \\ \mathrm{i}\frac{5}{8}\sqrt{10}A_{22} & -\sqrt{2}\left(2A_{29} - \frac{A_{22}}{8}\right) & -\mathrm{i}\left(A_{29} + \frac{A_{22}}{4}\right) & A_{216} & \mathrm{i}\left(-A_{27} + \frac{A_{21}}{4}\right) & -A_{25} - A_{26} \end{pmatrix} \tag{44}$$

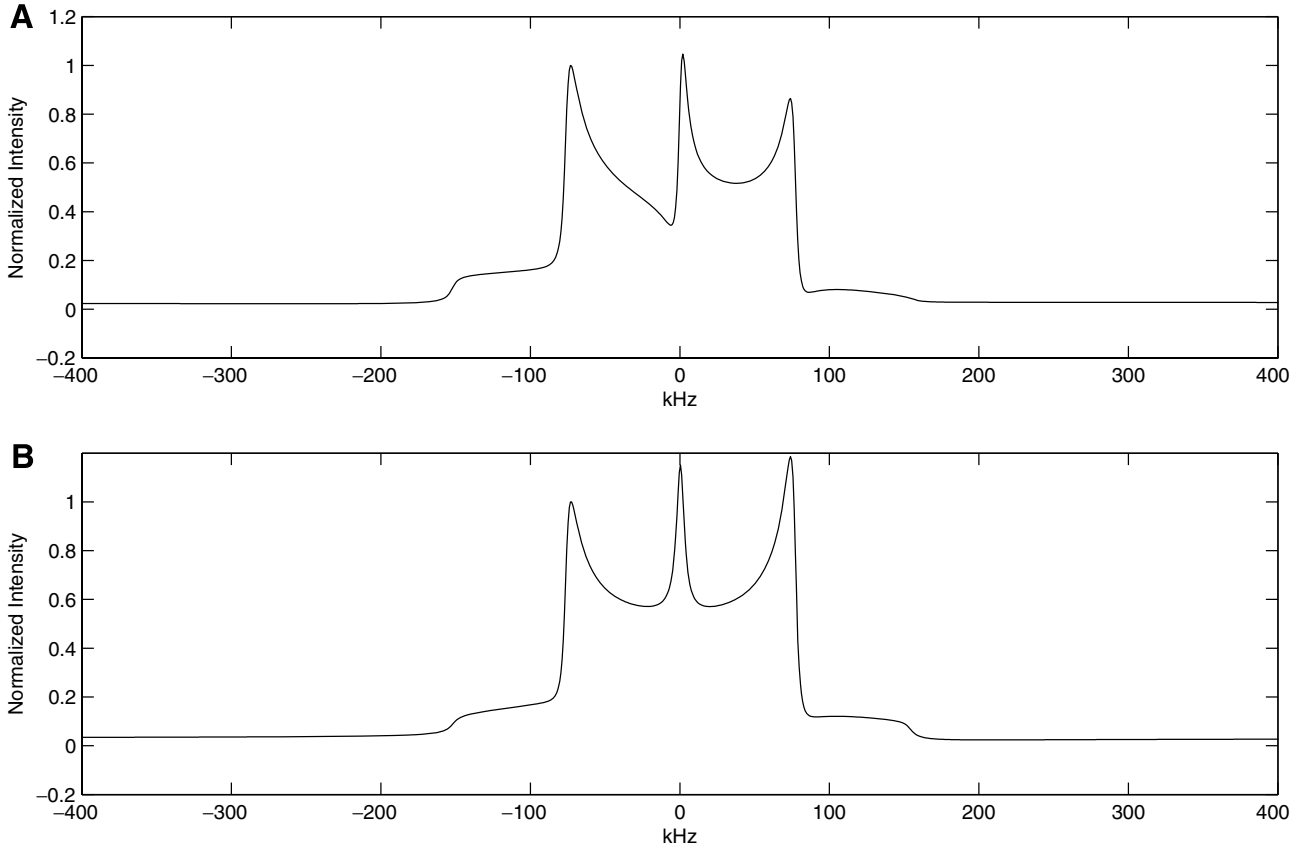

Fig. 8. (A) Simulated spectra acquired with an x, y cycle from Fig. 1 for a spin $I = 3/2$ system. (B) Simulated spectra using the pulse sequence in Fig. 1 with the eight-step phase cycling scheme given in Eq. (42) for a spin $I = 3/2$ system. In the simulation $\tau = 50\ \mu s$, $\alpha = 1\ \mu s$ and $dw = 0.25\ \mu s$.

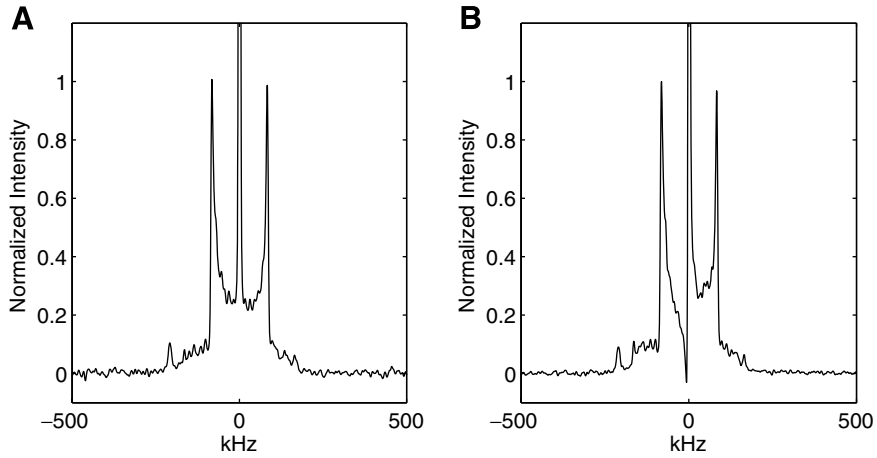

Fig. 9. (A) Experimental spectra of $NaNO_3$ acquired with a two-pulse quadrupolar echo with the eight-step phase cycling scheme given in Eq. (42). (B) Experimental spectra of $NaNO_3$ acquired with an x, y cycle and no phase cycling. In the experiment the $\pi/2$ pulse width was set to 1.2 μs and the τ spacing was set to 150 μs.

$$\rho^{\mathrm{AHT}}_{x,-y}(3\tau) = \begin{pmatrix} A_{25}+A_{26} & -\mathrm{i}\left(-A_{27}+\frac{A_{21}}{4}\right) & -A_{216} & \mathrm{i}\left(A_{29}+\frac{A_{22}}{4}\right) & \sqrt{2}\left(2A_{29}-\frac{A_{22}}{8}\right) & -\mathrm{i}\frac{5}{8}\sqrt{10}A_{22} \\ \mathrm{i}\left(-A_{27}+\frac{A_{21}}{4}\right) & A_{211}-A_{212} & -\mathrm{i}\left(-A_{210}+\frac{A_{23}}{4}\right) & -A_{213}-A_{214} & -\mathrm{i}\frac{7}{8}\sqrt{10}A_{22} & \sqrt{2}\left(2A_{29}+\frac{A_{22}}{8}\right) \\ -A_{216} & \mathrm{i}\left(-A_{210}+\frac{A_{23}}{4}\right) & -A_{215}+\frac{\sqrt{10}}{12}A_{22} & \mathrm{i}\frac{A_{24}}{4} & -A_{213}+A_{214} & \mathrm{i}\left(-A_{29}+\frac{A_{22}}{4}\right) \\ -\mathrm{i}\left(A_{29}+\frac{A_{22}}{4}\right) & -A_{213}-A_{214} & -\mathrm{i}\frac{A_{24}}{4} & -A_{215}-\frac{\sqrt{10}}{12}A_{22} & -\mathrm{i}\left(A_{210}+\frac{A_{23}}{4}\right) & -A_{28} \\ \sqrt{2}\left(2A_{29}-\frac{A_{22}}{8}\right) & \mathrm{i}\frac{7}{8}\sqrt{10}A_{22} & -A_{213}+A_{214} & \mathrm{i}\left(A_{210}+\frac{A_{23}}{4}\right) & -A_{211}-A_{212} & -\mathrm{i}\left(A_{27}+\frac{A_{21}}{4}\right) \\ \mathrm{i}\frac{5}{8}\sqrt{10}A_{22} & \sqrt{2}\left(2A_{29}+\frac{A_{22}}{8}\right) & -\mathrm{i}\left(-A_{29}+\frac{A_{22}}{4}\right) & -A_{28} & \mathrm{i}\left(A_{27}+\frac{A_{21}}{4}\right) & -A_{25}+A_{26} \end{pmatrix} \tag{45}$$

$$\rho^{\mathrm{AHT}}_{-x,y}(3\tau)=\begin{pmatrix} A_{25}+A_{26} & \mathrm{i}\left(-A_{27}+\frac{A_{21}}{4}\right) & -A_{216} & -\mathrm{i}\left(A_{29}+\frac{A_{22}}{4}\right) & \sqrt{2}\left(2A_{29}-\frac{A_{22}}{8}\right) & \mathrm{i}\frac{5}{8}\sqrt{10}A_{22} \\ -\mathrm{i}\left(-A_{27}+\frac{A_{21}}{4}\right) & A_{211}-A_{212} & \mathrm{i}\left(-A_{210}+\frac{A_{23}}{4}\right) & -A_{213}-A_{214} & \mathrm{i}\frac{7}{8}\sqrt{10}A_{22} & \sqrt{2}\left(2A_{29}+\frac{A_{22}}{8}\right) \\ -A_{216} & -\mathrm{i}\left(-A_{210}+\frac{A_{23}}{4}\right) & -A_{215}+\frac{\sqrt{10}}{12}A_{22} & -\mathrm{i}\frac{A_{24}}{4} & -A_{213}+A_{214} & \mathrm{i}\left(A_{29}-\frac{A_{22}}{4}\right) \\ \mathrm{i}\left(A_{29}+\frac{A_{22}}{4}\right) & -A_{213}-A_{214} & \mathrm{i}\frac{A_{24}}{4} & -A_{215}-\frac{\sqrt{10}}{12}A_{22} & \mathrm{i}\left(A_{210}+\frac{A_{23}}{4}\right) & -A_{28} \\ \sqrt{2}\left(2A_{29}-\frac{A_{22}}{8}\right) & -\mathrm{i}\frac{7}{8}\sqrt{10}A_{22} & -A_{213}+A_{214} & -\mathrm{i}\left(A_{210}+\frac{A_{23}}{4}\right) & -A_{211}-A_{212} & \mathrm{i}\left(A_{27}+\frac{A_{21}}{4}\right) \\ -\mathrm{i}\frac{5}{8}\sqrt{10}A_{22} & \sqrt{2}\left(2A_{29}+\frac{A_{22}}{8}\right) & \mathrm{i}\left(-A_{29}+\frac{A_{22}}{4}\right) & -A_{28} & -\mathrm{i}\left(A_{27}+\frac{A_{21}}{4}\right) & -A_{25}+A_{26} \end{pmatrix} \tag{46}$$

$$\rho^{\mathrm{AHT}}_{-x,-y}(3\tau)=\begin{pmatrix} A_{25}-A_{26} & \mathrm{i}\left(A_{27}+\frac{A_{21}}{4}\right) & A_{28} & -\mathrm{i}\left(-A_{29}+\frac{A_{22}}{4}\right) & -\sqrt{2}\left(2A_{29}+\frac{A_{22}}{8}\right) & \mathrm{i}\frac{5}{8}\sqrt{10}A_{22} \\ -\mathrm{i}\left(A_{27}+\frac{A_{21}}{4}\right) & A_{211}+A_{212} & \mathrm{i}\left(A_{210}+\frac{A_{23}}{4}\right) & A_{213}-A_{214} & \mathrm{i}\frac{7}{8}\sqrt{10}A_{22} & -\sqrt{2}\left(2A_{29}-\frac{A_{22}}{8}\right) \\ A_{28} & -\mathrm{i}\left(A_{210}+\frac{A_{23}}{4}\right) & A_{215}+\frac{\sqrt{10}}{12}A_{22} & -\mathrm{i}\frac{A_{24}}{4} & A_{213}+A_{214} & -\mathrm{i}\left(A_{29}+\frac{A_{22}}{4}\right) \\ \mathrm{i}\left(-A_{29}+\frac{A_{22}}{4}\right) & A_{213}-A_{214} & \mathrm{i}\frac{A_{24}}{4} & A_{215}-\frac{\sqrt{10}}{12}A_{22} & \mathrm{i}\left(-A_{210}+\frac{A_{23}}{4}\right) & A_{216} \\ -\sqrt{2}(2A_{29}+\frac{A_{22}}{8}) & -\mathrm{i}\frac{7}{8}\sqrt{10}A_{22} & A_{213}+A_{214} & -\mathrm{i}\left(-A_{210}+\frac{A_{23}}{4}\right) & A_{212}-A_{211} & \mathrm{i}\left(-A_{27}+\frac{A_{21}}{4}\right) \\ -\mathrm{i}\frac{5}{8}\sqrt{10}A_{22} & -\sqrt{2}\left(2A_{29}-\frac{A_{22}}{8}\right) & \mathrm{i}\left(A_{29}+\frac{A_{22}}{4}\right) & A_{216} & -\mathrm{i}\left(-A_{27}+\frac{A_{21}}{4}\right) & -A_{25}-A_{26} \end{pmatrix} \tag{47}$$

$$\rho^{\mathrm{AHT}}_{y,x}(3\tau)=\begin{pmatrix} A_{25}+A_{26} & A_{27}-\frac{A_{21}}{4} & A_{216} & -A_{29}-\frac{A_{22}}{4} & \sqrt{2}\left(2A_{29}-\frac{A_{22}}{8}\right) & -\frac{5}{8}\sqrt{10}A_{22} \\ A_{27}-\frac{A_{21}}{4} & A_{211}-A_{212} & A_{210}-\frac{A_{23}}{4} & A_{213}+A_{214} & \frac{7}{8}\sqrt{10}A_{22} & \sqrt{2}\left(2A_{29}+\frac{A_{22}}{8}\right) \\ A_{216} & A_{210}-\frac{A_{23}}{4} & -A_{215}+\frac{\sqrt{10}}{12}A_{22} & \frac{A_{24}}{4} & A_{213}-A_{214} & A_{29}-\frac{A_{22}}{4} \\ -A_{29}-\frac{A_{22}}{4} & A_{213}+A_{214} & \frac{A_{24}}{4} & -A_{215}-\frac{\sqrt{10}}{12}A_{22} & -A_{210}-\frac{A_{23}}{4} & A_{28} \\ \sqrt{2}\left(2A_{29}-\frac{A_{22}}{8}\right) & \frac{7}{8}\sqrt{10}A_{22} & A_{213}-A_{214} & -A_{210}-\frac{A_{23}}{4} & -A_{211}-A_{212} & -A_{27}-\frac{A_{21}}{4} \\ -\frac{5}{8}\sqrt{10}A_{22} & \sqrt{2}\left(2A_{29}+\frac{A_{22}}{8}\right) & A_{29}-\frac{A_{22}}{4} & A_{28} & -A_{27}-\frac{A_{21}}{4} & -A_{25}+A_{26} \end{pmatrix} \tag{48}$$

$$\rho^{\mathrm{AHT}}_{y,-x}(3\tau)=\begin{pmatrix} A_{25}-A_{26} & -A_{27}-\frac{A_{21}}{4} & -A_{28} & A_{29}-\frac{A_{22}}{4} & -\sqrt{2}\left(2A_{29}+\frac{A_{22}}{8}\right) & -\frac{5}{8}\sqrt{10}A_{22} \\ -A_{27}-\frac{A_{21}}{4} & A_{211}+A_{212} & -A_{210}-\frac{A_{23}}{4} & -A_{213}+A_{214} & \frac{7}{8}\sqrt{10}A_{22} & -\sqrt{2}\left(2A_{29}-\frac{A_{22}}{8}\right) \\ -A_{28} & -A_{210}-\frac{A_{23}}{4} & A_{215}+\frac{\sqrt{10}}{12}A_{22} & \frac{A_{24}}{4} & -A_{213}-A_{214} & -A_{29}-\frac{A_{22}}{4} \\ A_{29}-\frac{A_{22}}{4} & -A_{213}+A_{214} & \frac{A_{24}}{4} & A_{215}-\frac{\sqrt{10}}{12}A_{22} & A_{210}-\frac{A_{23}}{4} & -A_{216} \\ -\sqrt{2}\left(2A_{29}+\frac{A_{22}}{8}\right) & \frac{7}{8}\sqrt{10}A_{22} & -A_{213}-A_{214} & A_{210}-\frac{A_{23}}{4} & -A_{211}+A_{212} & A_{27}-\frac{A_{21}}{4} \\ -\frac{5}{8}\sqrt{10}A_{22} & -\sqrt{2}\left(2A_{29}-\frac{A_{22}}{8}\right) & -A_{29}-\frac{A_{22}}{4} & -A_{216} & A_{27}-\frac{A_{21}}{4} & -A_{25}-A_{26} \end{pmatrix} \tag{49}$$

$$\rho^{\mathrm{AHT}}_{-y,x}(3\tau)=\begin{pmatrix} A_{25}-A_{26} & A_{27}+\frac{A_{21}}{4} & -A_{28} & -A_{29}+\frac{A_{22}}{4} & -\sqrt{2}\left(2A_{29}+\frac{A_{22}}{8}\right) & \frac{5}{8}\sqrt{10}A_{22} \\ A_{27}+\frac{A_{21}}{4} & A_{211}+A_{212} & A_{210}+\frac{A_{23}}{4} & -A_{213}+A_{214} & -\frac{7}{8}\sqrt{10}A_{22} & -\sqrt{2}\left(2A_{29}-\frac{A_{22}}{8}\right) \\ -A_{28} & A_{210}+\frac{A_{23}}{4} & A_{215}+\frac{\sqrt{10}}{12}A_{22} & -\frac{A_{24}}{4} & -A_{213}-A_{214} & A_{29}+\frac{A_{22}}{4} \\ -A_{29}+\frac{A_{22}}{4} & -A_{213}+A_{214} & -\frac{A_{24}}{4} & A_{215}-\frac{\sqrt{10}}{12}A_{22} & -A_{210}+\frac{A_{23}}{4} & -A_{216} \\ -\sqrt{2}\left(2A_{29}+\frac{A_{22}}{8}\right) & -\frac{7}{8}\sqrt{10}A_{22} & -A_{213}-A_{214} & -A_{210}+\frac{A_{23}}{4} & -A_{211}+A_{212} & -A_{27}+\frac{A_{21}}{4} \\ \frac{5}{8}\sqrt{10}A_{22} & -\sqrt{2}\left(2A_{29}-\frac{A_{22}}{8}\right) & A_{29}+\frac{A_{22}}{4} & -A_{216} & -A_{27}+\frac{A_{21}}{4} & -A_{25}-A_{26} \end{pmatrix} \tag{50}$$

$$\rho^{\mathrm{AHT}}_{-y,-x}(3\tau)=\begin{pmatrix} A_{25}+A_{26} & -A_{27}+\frac{A_{21}}{4} & A_{216} & A_{29}+\frac{A_{22}}{4} & \sqrt{2}\left(2A_{29}-\frac{A_{22}}{8}\right) & \frac{5}{8}\sqrt{10}A_{22} \\ -A_{27}+\frac{A_{21}}{4} & A_{211}-A_{212} & -A_{210}+\frac{A_{23}}{4} & A_{213}+A_{214} & -\frac{7}{8}\sqrt{10}A_{22} & \sqrt{2}\left(2A_{29}+\frac{A_{22}}{8}\right) \\ A_{216} & -A_{210}+\frac{A_{23}}{4} & -A_{215}+\frac{\sqrt{10}}{12}A_{22} & -\frac{A_{24}}{4} & A_{213}-A_{214} & -A_{29}+\frac{A_{22}}{4} \\ A_{29}+\frac{A_{22}}{4} & A_{213}+A_{214} & -\frac{A_{24}}{4} & -A_{215}-\frac{\sqrt{10}}{12}A_{22} & A_{210}+\frac{A_{23}}{4} & A_{28} \\ \sqrt{2}\left(2A_{29}-\frac{A_{22}}{8}\right) & -\frac{7}{8}\sqrt{10}A_{22} & -A_{213}+A_{214} & -A_{210}-\frac{A_{23}}{4} & -A_{211}-A_{212} & A_{27}+\frac{A_{21}}{4} \\ \frac{5}{8}\sqrt{10}A_{22} & \sqrt{2}\left(2A_{29}+\frac{A_{22}}{8}\right) & -A_{29}+\frac{A_{22}}{4} & A_{28} & A_{27}+\frac{A_{21}}{4} & -A_{25}+A_{26} \end{pmatrix} \tag{51}$$

Table 2
Constants used in the expressions for the density matrices of a spin $I = 5/2$ nuclear spin system

A_{21}	$\frac{\sqrt{5}}{196}[153 + 244\cos(a) - 5\cos(2a)]$
A_{22}	$\frac{6\sqrt{10}}{49}\sin^4(b)$
A_{23}	$\frac{1}{98\sqrt{2}}[477 + 260\cos(a) + 47\cos(2a)]$
A_{24}	$\frac{3}{14}[-9 - 20\cos(a) + \cos(2a)]$
A_{25}	$\frac{5}{784}[-129 + 116\cos(a) + 13\cos(2a)]$
A_{26}	$\frac{5}{784}\left[52\sqrt{14}\sin(a) + 2\sqrt{14}\sin(2a)\right]$
A_{27}	$\frac{\sqrt{5}}{784}\left[36\sqrt{14}\sin(a) + 10\sqrt{14}\sin(2a)\right]$
A_{28}	$\frac{1}{784}\left[-153\sqrt{10} + 120\sqrt{10}\cos(a) + 33\sqrt{10}\cos(2a) + 44\sqrt{35}\sin(a) + 6\sqrt{35}\sin(2a)\right]$
A_{29}	$\frac{6\sqrt{35}}{98}\sin^3(b)\cos(b)$
A_{210}	$\frac{1}{784}\left[180\sqrt{7}\sin(a) - 34\sqrt{7}\sin(2a)\right]$
A_{211}	$\frac{1}{784}[-447 + 540\cos(a) - 93\cos(2a)]$
A_{212}	$\frac{1}{784}\left[100\sqrt{14}\sin(a) - 22\sqrt{14}\sin(2a)\right]$
A_{213}	$\frac{3}{392}\sin(a)\left[-2\sqrt{7}(-15 + \cos(a))\right]$
A_{214}	$\frac{3 * 21\sqrt{2}}{392}\sin^2(a)$
A_{215}	$\frac{2\sqrt{14}}{49}[5\sin(a) + \sin(2a)]$
A_{216}	$\frac{\sqrt{5}}{392}\sin(b)\left[50\sqrt{7}\cos(\sqrt{b}) + 6\sqrt{7}\cos(3b) + 3\sqrt{2}(51\sin\left(\sqrt{b}\right) + 11\sin(3\sqrt{b}))\right]$

In the above table, $a = \sqrt{14}W$, $b = \frac{7}{2}W$ and $W = \frac{12\alpha\omega_Q}{\pi}$.

For the expressions in the density matrices for spin 5/2, the constants are given in Table 2. In each of the density matrices exists double-, triple-, fourth- and fifth-order quantum coherences. Careful inspection of the tabulated constants reveals that these terms result from the evolution of the spin system during the RF pulses. In the limiting case of ideal δ-function pulses, these coherence are all seen to vanish. For any given cycle, the constants that compose the first-order coherence A_{27}, A_{21}, A_{210}, A_{23}, A_{24} are both odd and even functions. The sum of odd and even functions, as discussed above for spin $I = 3/2$, will result in a slightly asymmetric spectrum for each cycle.

Using the same approach for spin $I = 3/2$ and $I = 1$, we add or subtract the cycles to cancel these deleterious terms. The result for the echoes forming on the x axis relative to the receiver is given by

$$S_x^{\mathrm{AHT}}(3\tau) = \rho_{y,x}^{\mathrm{AHT}}(3\tau) + \rho_{y,-x}^{\mathrm{AHT}}(3\tau) - \rho_{-y,x}^{\mathrm{AHT}}(3\tau) - \rho_{-y,-x}^{\mathrm{AHT}}(3\tau) \tag{52}$$

which reduces to

$$S_x^{\mathrm{AHT}}(3\tau) = \begin{pmatrix} 0 & -A_{21} & 0 & -A_{22} & 0 & -\frac{5}{2}\sqrt{10}A_{22} \\ -A_{21} & 0 & -A_{23} & 0 & \frac{7}{2}\sqrt{10}A_{22} & 0 \\ 0 & -A_{23} & 0 & A_{24} & 0 & -A_{22} \\ -A_{22} & 0 & A_{24} & 0 & -A_{23} & 0 \\ 0 & \frac{7}{2}\sqrt{10}A_{22} & 0 & -A_{23} & 0 & -A_{21} \\ -\frac{5}{2}\sqrt{10}A_{22} & 0 & -A_{22} & 0 & -A_{21} & 0 \end{pmatrix} \tag{53}$$

For the echoes occurring on the y axis relative to the receiver one finds

$$S_y^{\mathrm{AHT}}(3\tau) = \rho_{x,y}^{\mathrm{AHT}}(3\tau) + \rho_{x,-y}^{\mathrm{AHT}}(3\tau) - \rho_{-x,y}^{\mathrm{AHT}}(3\tau) - \rho_{-x,-y}^{\mathrm{AHT}}(3\tau), \tag{54}$$

which reduces to

$$S_y^{\mathrm{AHT}}(3\tau) = \begin{pmatrix} 0 & -\mathrm{i}A_{21} & 0 & \mathrm{i}A_{22} & 0 & -\mathrm{i}\frac{5}{2}\sqrt{10}A_{22} \\ \mathrm{i}A_{21} & 0 & -\mathrm{i}A_{23} & 0 & -\mathrm{i}\frac{7}{2}\sqrt{10}A_{22} & 0 \\ 0 & \mathrm{i}A_{23} & 0 & \mathrm{i}A_{24} & 0 & \mathrm{i}A_{22} \\ -\mathrm{i}A_{22} & 0 & -\mathrm{i}A_{24} & 0 & -\mathrm{i}A_{23} & 0 \\ 0 & \mathrm{i}\frac{7}{2}\sqrt{10}A_{22} & 0 & \mathrm{i}A_{23} & 0 & -\mathrm{i}A_{21} \\ \mathrm{i}\frac{5}{2}\sqrt{10}A_{22} & 0 & -\mathrm{i}A_{22} & 0 & \mathrm{i}A_{21} & 0 \end{pmatrix} \tag{55}$$

The triple- and fifth-order quantum coherences terms do not evolve under the secular quadrupolar Hamiltonian and are hence constants of the motion. The constants that compose the first-order coherences A_{21}, A_{23}, A_{24} are now all only even functions. Thus, we suppress the odd functions and remove the spectral distortion by phase cycling to first-order of the Magnus expansion. In the limiting case of $\alpha \to 0$, the density matrices at 3τ calculated above reduce to

$$S_x(3\tau) = -4I_x \tag{56}$$

and

$$S_y(3\tau) = 4I_y \tag{57}$$

This corresponds to the case of perfect refocusing of the spin magnetization and is what one would expect in the case of δ-function RF pulses.

We simulated the spectra for a spin $I = 5/2$ ensemble with $2\alpha = 1$ μs, $\tau = 150$ μs and $\omega_Q = 80$ kHz. The simulation shown in Fig. 10 illustrates five peaks corresponding to the five transitions involving six energy levels of spin $I = 5/2$. Fig. 10A shows the results when an x, y cycle is applied. Our results in Fig. 10A indicate that the spectra is skewed, and Fig. 10B shows that the distortion is not removed by the phase cycling scheme that appeared to work for $I = 1$ and $I = 3/2$, given in Eq. (42). We empirically found that the subtraction of x, y to $-x$, y appears to remove the distortion present in the spectra, shown in Fig. 10C. The zeroth-order analysis presented for $I = 5/2$ does not predict this behavior because the first-order term, which is proportional to τ^2, is larger than the zeroth-order term, which is proportional to α^2.

3. Experiment

We investigated the effects of finite pulse width artifacts and the correction one would expect to achieve by implementing the phase cycling scheme outlined in the previous section on a powdered sample of $NaNO_3$ containing $I = 3/2$ nuclei and a second sample of $AlCl_3$ containing $I = 5/2$ nuclei. For the sample containing spin $I = 3/2$ nuclei, we used a packed powdered sample of $NaNO_3$ in a glass tube having an outer diameter of approximately 2 mm. The experiments for this sample were performed using a home-built probe tuned to the Larmor frequency of Na, which was approximately 47.47 MHz in our magnet. The $AlCl_3$ samples were packed into a 7 mm MAS rotor, and the experiments were run using a Doty Scientific probe fitted with capacitors capable of handling high RF power. The experiments for both samples were performed using an Apollo Tecmag spectrometer at room temperature. For each nucleus, the radio frequency pulses were tuned by using well known techniques from multiple-pulse NMR [11].

Fig. 9 shows the experimental quadrupolar echo spectra for the $NaNO_3$ sample acquired with a pulse width of 1.2 μs with and without the phase cycling scheme given in the previous section. The experimental spectra shown were acquired using pulse spacing of 150 μs. The data show that without the phase cycling scheme an asymmetry is present in the spectra. This is due to the presence of both odd and even functions in the SQ coherences of the density matrix well predicted by the spectral simulations shown in Fig. 8. The asymmetry is expected to vanish in the limiting case of $\alpha \to 0$, as shown in the previous section. With the phase cycling scheme implemented, we produce symmetric spectra as predicted by AHT and shown in the simulation results. The sharp peak in the middle of the spectra is due to the $-1/2$ to $1/2$ transition for spin 3/2 nuclei, and the small peak approximately 213 kHz off resonance we believe results from copper in the RF coil that could not be phase cycled away.

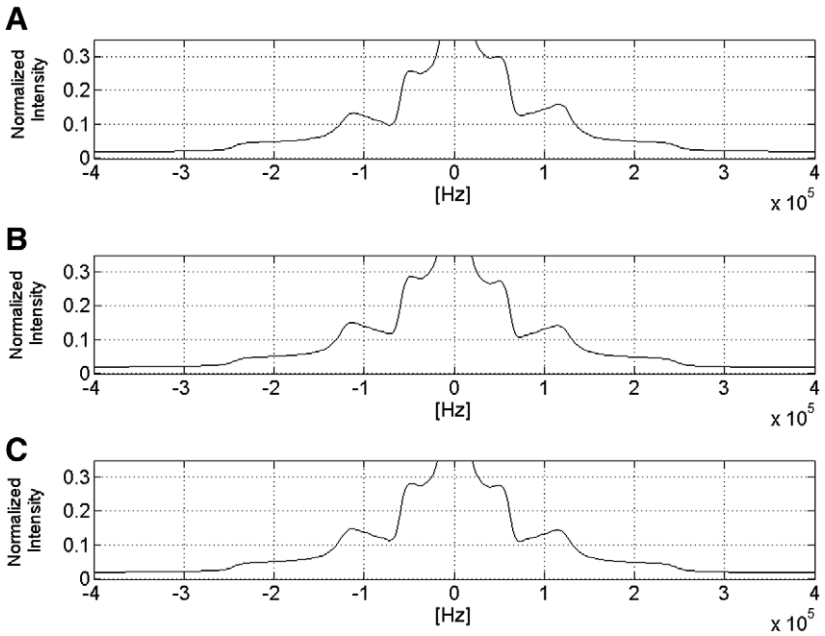

Fig. 10. (A) Simulated spectra acquired with the eight-step phase cycling scheme given in Eq. (42) for a spin $I = 5/2$ system. (B) Simulated spectra using an x, y cycle for a spin $I = 5/2$ system. In the simulation $\tau = 50$ μs, $\alpha = 1$ μs and dw = 0.25 μs.

While it is expected that the phase cycling scheme introduced in this work should correct for the finite pulse width artifact of an asymmetric spectrum, we experimentally find that the artifacts are not suppressed as well for $I = 5/2$ as that found for spin $I = 1$ [20] and in Fig. 9 for spin $I = 3/2$. For spin $I = 5/2$, Fig. 11 highlights the experimental data acquired at 1.1 μs with and without the artifact suppressing phase cycling scheme. The data indicate that with the proposed phase cycling scheme shown in Eq. (42), the symmetry of the spectra is recovered to some extent. With shorter pulse spacings, the spectra may be further distorted due to the ringdown of the RF coil. However, such artifacts associated with short echo times may be removed by implementing a well-defined phase cycling scheme as discussed by others [21,22].

4. Conclusion

In this work, we investigated controlling the dynamics of $I = 1$, $I = 3/2$ and $I = 5/2$ nuclei by AHT. A numerical study of a well known two-pulse cycle showed that first-order AHT predicts the spin dynamics for spin $I = 1$ over a large bandwidth, and for relatively large pulse spacings. For spin $I = 3/2$ and $I = 5/2$ nuclei, AHT predicts the dynamics of the spin system only for short τ, small bandwidths and short RF pulses. To probe our ability to control the coherent evolution of a quadrupolar spin system by AHT, we studied a phase cycling scheme shown to suppress spectral artifacts associated with finite pulse widths [20]. Experimentally it was demonstrated that the artifacts can be suppressed only for nu-

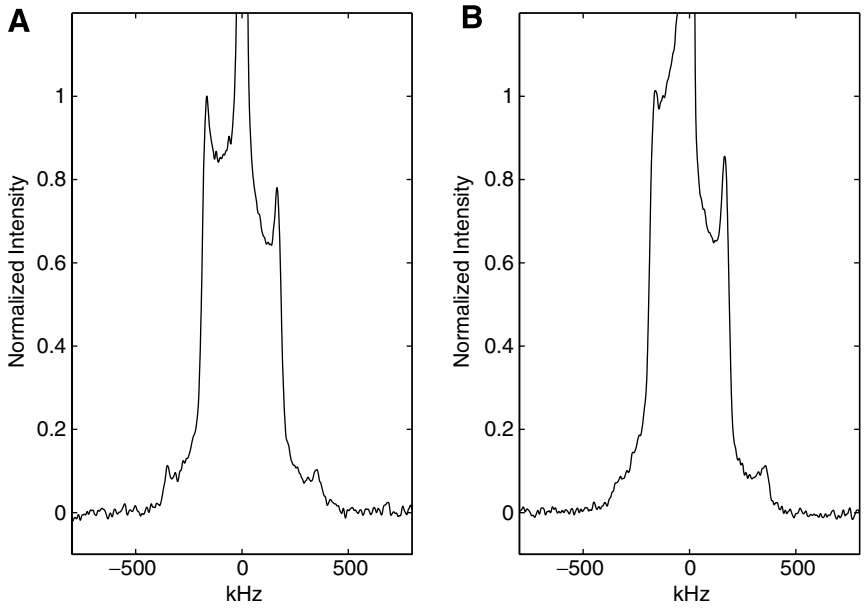

Fig. 11. (A) Experimental spectra of $AlCl_3$ acquired with a two-pulse quadrupolar echo and with the eight step phase cycling scheme given in Eq. (42). (B) Experimental spectra of $AlCl_3$ acquired with only an x, y cycle and no phase cycling. In the experiment, the $\pi/2$ pulse width was set to 1.1 μs and the τ spacing was set to 150 μs.

clei having a low quadrupolar moment due to the contribution of non-negligible higher order terms in the Magnus expansion. While this work focused on a simple two-pulse sequence, the efficiency of AHT is intimately tied to this cycle. More efficient truncation of the Magnus expansion is expected for quadrupolar spins by exploiting the symmetry properties of a pulse sequence [23].

Acknowledgments

E.S. Mananga acknowledges support by The City University of New York (CUNY), Graduate Center Alliance for Graduate Education in the Professoriate (AGEP) program funded by the National Science Foundation. We thank Professor Joel Gersten of the City College of CUNY for useful discussions. We would also thank Professor Ruth Stark of City College of CUNY for her recent donation of a Varian UNITY NMR spectrometer and several solid state NMR probes that assisted us in this investigation.

References

[1] I.I. Rabi, S. Millman, P. Kusch, J.R. Zacharias, The Molecular beam resonance method for measuring nuclear magnetic moments: the magnetic moments of 3Li6, 3Li7 and 9F19, Phys. Rev. 55 (1939) 526–535.
[2] E.L. Hahn, Spin echoes, Phys. Rev. 80 (1950) 580–594.
[3] W.S. Warren, Effects of pulse shaping in laser spectroscopy and nuclear magnetic resonance, Science 242 (1988) 878–884.
[4] C. Counsell, M.H. Levitt, R.R. Ernst, Analytical theory of composite pulses, J. Magn. Res. 63 (1985) 133–141.
[5] R. Tycko, E. Schneider, A. Pines, Broadband population inversion in solid state NMR, J. Chem. Phys. 81 (1984) 680–688.
[6] E.M. Fortunato, M.A. Pravia, N. Boulant, G. Teklemariam, D.G. Cory, T. Havel, Design of strongly modulating pulses to implement precise effective Hamiltonians for quantum information processing, J. Chem. Phys. 116 (2002) 7599–7606.
[7] H. Geen, R. Freeman, Band-selective radiofrequency pulses, J. Magn. Res. 93 (1991) 93–141.
[8] B. Ewing, S.J. Glaser, G.P. Drobny, Experimental demonstrations of shaped pulses for narrowband inversion of uncoupled and coupled systems, J. Magn. Res. 98 (1992) 381–387.
[9] U. Haeberlen, J.S. Waugh, Coherent averaging effects in magnetic resonance, Phys. Rev. 175 (1968) 453–467.
[10] M.M. Maricq, Application of average Hamiltonian theory to the NMR of solids, Phys. Rev. B 25 (1982) 6622–6632.
[11] B.C. Gerstein, C.R. Dybowski, Transient Techniques in NMR of Solids, Academic Press, Inc., 1985.
[12] I. Solomon, Multiple echoes in solids, Phys. Rev. 110 (1958) 6165.
[13] P.P. Man, Determination of spin-5/2 quadrupolar coupling with two-pulse sequences, J. Magn. Reson. 2 (1993) 165–180.
[14] P.P. Man, Study of a spin-3/2 system by a quadrupolar-echo sequence: suppression of spurious signals, Solid State NMR 1 (1992) 149–158.
[15] J. Haase, E. Oldfield, Spin echo behavior of nonintegral-spin quadrupolar nuclei in inorganic solids, J. Magn. Res. A 101 (1993) 30–40.
[16] O.A. Nagel, M.E. Ramia, C.A. Martin, Density matrix calculation of spin 5/2 pure nuclear quadrupole resonance echoes, Phys. A 218 (1995) 487–506.
[17] L. Pandey, M. Kotecha, D.G. Hughes, Calculation of pulsed NMR signal in $I = 3/2$ quadrupolar spin system, Solid State Nuclear Magn. Reson. 16 (2000) 261–269.
[18] Yves Dumazy, Jean-Paul Amoureux, Christian Fernandez, Theoretical and experimental study of quadrupolar echoes in solid state NMR, Mol. Phys. 90 (1997) 959.
[19] L.I. Schiff, Quantum Mechanics, McGraw-Hill, New York, 1968.
[20] E.S. Mananga, Y.S. Rumala, G.S. Boutis, Finite pulse width artifact suppression in spin-1 quadrupolar echo spectra by phase cycling, J. Magn. Reson. 181 (2006) 296–303.
[21] I. Furo, N. Hedin, Noise reduction in quadrupolar echo spectra at short echo times, J. Magn. Reson. 152 (2001) 214–216.
[22] A.D. Ronemus, R.L. Vold, R.R. Vold, Deuterium quadrupole echo NMR spectroscopy II. Artifact suppression, J. Magn. Reson. 70 (1986) 416–426.
[23] U. Haeberlen, High Resolution NMR in Solids: Selective Averaging, Academic Press, New York, 1976.